molecules

MDPI

Article

A Simple Analysis of the Second (Extra) Disulfide Bridge of V_HHs

Carla Martins [1,2], Fabrice Gardebien [2], Aravindan Arun Nadaradjane [2], Julien Diharce [1,*] and Alexandre G. de Brevern [1,2,*]

[1] Université Paris Cité and Université de la Réunion and Université des Antilles, INSERM, BIGR, DSIMB, F-75015 Paris, France; cmartins@insa-toulouse.fr
[2] Université Paris Cité and Université de la Réunion and Université des Antilles, INSERM, BIGR, DSIMB, F-97715 Saint Denis Messag, France; fabrice.gardebien@univ-reunion.fr (F.G.); aravindan.nadaradjane@univ-reunion.fr (A.A.N.)
* Correspondence: julien.diharce@u-paris.fr (J.D.); alexandre.debrevern@univ-paris-diderot.fr (A.G.d.B.)

Abstract: Camelids produce a special type of antibody, known as V_HHs, that has lost the V_L domain, providing a more optimised V_H domain. This particular highly stable antibody domain has interesting properties for biotechnological development. Ordinarily, those molecules possess only one disulphide bridge, but surprisingly, at least a quarter of these V_HHs have a second one. Curiously, this does not seem to be essential for the stability and the function of this domain. In an attempt to characterise precisely the role and impact of this disulphide bridge at the molecular level, several in silico mutants of a V_HH were created to disrupt this second disulphide bridge and those systems were submitted to molecular dynamics simulation. The loss of the second disulphide bridge leads to an increase in the flexibility of CDR1 and CDR3 and an unexpected rigidification of CDR2. Local conformational analysis shows local differences in the observed protein conformations. However, in fact, there is no exploration of new conformations but a change in the equilibrium between the different observed conformations. This explains why the interaction of V_HHs is not really affected by the presence or absence of this second bridge, but their rigidity is slightly reduced. Therefore, the additional disulphide bridge does not seem to be an essential part of V_HHs function.

Keywords: secondary structure; sequence structure relationship; structural alphabet; molecular dynamics; antibodies; frameworks

Citation: Martins, C.; Gardebien, F.; Nadaradjane, A.A.; Diharce, J.; de Brevern, A.G. A Simple Analysis of the Second (Extra) Disulfide Bridge of V_HHs. *Molecules* **2024**, *29*, 4863. https://doi.org/10.3390/molecules29204863

Academic Editors: Anna Marabotti and Takeshi Kikuchi

Received: 30 July 2024
Revised: 8 October 2024
Accepted: 10 October 2024
Published: 14 October 2024

1. Introduction

Immunoglobulins (Ig) are large Y-shaped proteins used by the immune system to identify and neutralize antigens by direct interactions. They are composed of various different types of Igs, the most classical being IgG. Members of this family are composed of two heavy (with C_H1, C_H2, C_H3, and V_H domains) and two light chains (with C_L and V_L, domains, see Figure 1C,E). They are found in all mammals (see Figure 1A), but the members of the family *Camelidae* (including *Lama glama*, *Camelus bactrianus*, *Camelus dromedarius*, and *Vicugna pacos*) also have a supplementary modified variety of IgG which completely lacks (i) light chains (no C_L and V_L domains) and (ii) the C_H1 domain (see Figure 1B) [1]. They were named heavy-chain-only antibodies (HCAb, see Figure 1D,F) [2,3] and they are important for camelid newborns [4]. In HCAbs, the deletion of the splicing consensus sequence in their mRNA results in the absence of the heavy chain C_H1 domain [5,6]. In the absence of the V_L domain, the formerly hydrophobic V_H-V_L interface has evolved to adapt to the hydrophilic environment [5,7]. The final VH domain of these HCAbs is called V_HH (or nanobody [8]) [9].

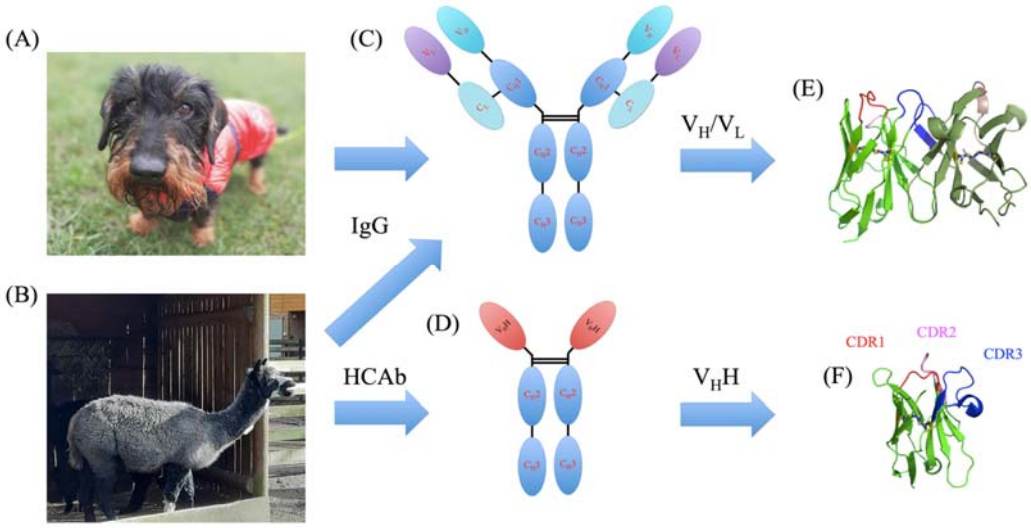

Figure 1. Comparison of V_H/V_L and V_HH domains. (**A**) A classical wirehaired dachshund named Snoopy that has classical IgGs and (**B**) a *Vicugna pacos* from Krakow Zoo that also has HCAbs. Schematic representation of (**C**) IgG and (**D**) HCAb with C_H1, C_H2, C_H3, V_H, C_L, V_H, and V_HH domains with a 3D representation with CDR1 in red, CDR2 in pink, and CDR3 in blue colours for (**E**) V_H/V_L and (**F**) V_HH. Three-dimensional visualization was carried out with PyMOL [10–12].

V_H, V_L, and V_HH domains are composed of four framework regions (FRs), highly conserved; they form a classic scaffold composed mainly of β-sheets. Three Complementary Determinant Regions (CDRs) link them; those regions are highly variable in terms of sequence as they provide the specificity that allows for the recognition of the epitope by the paratope. V_HH domains are half the volume of the V_H-V_L complex. The loss of binding surface area is compensated by the increase in CDR length (particularly CDR3); thus, they provide certain particular conformations less present in IgGs [13]. V_HHs have interesting experimental properties because they are easier to over-express than classical IgGs, e.g., in heterologous expression systems as *E. coli*, plant, or by phage display [14–17]. They have high thermal tolerance [18,19], induced by intramolecular interactions between the CDR3 and the FR2 region [20]. Their small size, ease of expression, and unique biochemical and biophysical properties have made V_HH the harbingers of biotechnological tools used in healthcare therapeutics and diagnostics. Several innovative V_HH drugs have been developed, e.g., Caplacizumab® against acquired Thrombotic Thrombocytopenic Purpura [21–23], Ozoralizumab (Nanozora®) against rheumatoid arthritis [24,25], or Ciltacabtagene autoleucel (CARVYKTI®) against refractory/relapsed multiple myeloma [26,27].

The disulfide bridges of immunoglobulins were characterized decades ago; they are numerous and are found mainly within each domain [28–30]. The domains (C_Hs, C_L, V_L, and V_H) of IgGs most often have one characteristic and a conserved disulphide bridge [31]. These bridges are highly important in V_H and V_L domains [32]. Disulphide bridges are also found between heavy chains and between heavy and light chains [33]. Non-classical disulphide bond structures were first identified in IgG_4 and later in IgG_2 antibodies, but they remain highly rare [34].

Analysis of V_HHs has revealed the presence of other additional disulphide bridges not generally found in antibody V_H domains [35–37] (see Figure 2). Different types of additional disulphide bridges are observed in V_HH sequences and almost always involve CDR1, more rarely FR2 or CDR2, and most commonly CDR3 [38–40]. However, the majority of these studies focus only on cysteine patterns, not disulphide bond evidence. We therefore draw your attention to an example that is representative of the majority of the Protein Data Bank's V_HHs with an additional disulphide bond. It is found between CDR1 and CDR3 (IMGT positions C33–C102) [36,41]. Sequence and structure studies highlight that this second disulfide bridge, between CDR1 and CDR3, is found in a quarter of V_HHs [13,42,43].

It is the most common of the extra bridges; others are much rarer. Surprisingly, it seems that they are not as essential as could be expected [44–46].

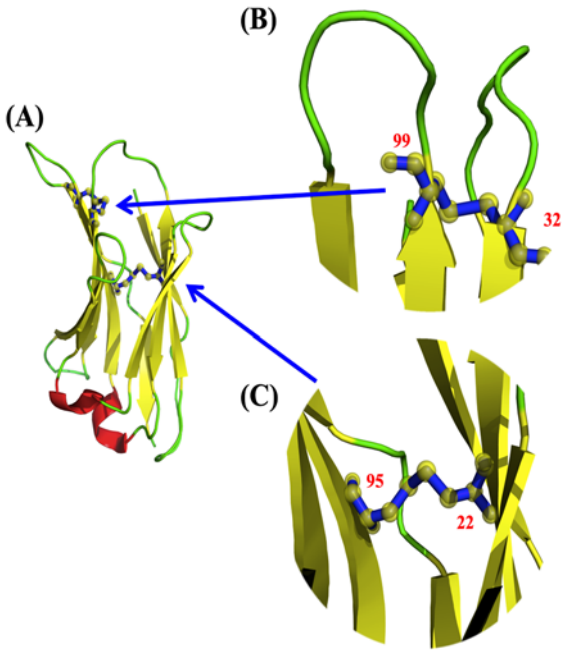

Figure 2. V_HH disulphide bridges. (**A**) V_HH PDB id 1YC7 [35], with the two disulphide bridges, (**B**) the supplementary disulphide bridge (positions 32 and 99), and (**C**) the canonical disulphide bridge (positions 22 and 95). Visualization was carried out with PyMOL [10–12].

Disulphide bridges are particularly interesting from a structural perspective and are often seen as essential for maintaining protein topology [47]. However, this is not always the case [48], raising specific questions in the context of these antibodies. An experimental study even showed that V_HH with or without this second disulphide bridge had the same characteristics in terms of stability and affinity [44], while previous conclusions considered that its presence increases those properties [49].

Our research specifically investigates the existence of this not-so-rare additional disulphide bridge present between the hypervariable regions, CDRs. We therefore carried out in silico mutagenesis in four different experiments: (i) replacing the first Cysteine with an Alanine, (ii) then just the second Cysteine with an Alanine, (iii) then both Cysteines with Alanines, and finally (iv) by substituting Glycines for Cysteines. These five systems (wild types and four series of variants) are analysed comparatively by molecular dynamics simulations. Classical (RMSf) and innovative approaches (Protein Blocks [50] with PBxplore software [51]) are used. Our results shed light on the lack of role of this second disulphide bridge. In fact, its absence does not seem to affect their conformations and affects their dynamical behaviours only slightly. Although not intuitive at first, the results are consistent with the experimental results.

2. Results

2.1. Systems

While almost all V_HH share a common canonical disulphide bond (found in this V_HH at positions C23-C104), approximately only one-quarter have a second disulphide bond between CDR1 and CDR3 (found in this V_HH at positions C32–C99). To elucidate its possible role in the antigenic binding of V_HH by stabilizing the CDR3 loop, e.g., reducing the entropic penalty, a V_HH that recognizes the surface glycoprotein carbohydrates of trypanosomes, parasites/hematophagous insects responsible for infections, the trypanosomiases (PDB ID 1YC7 [35], see Figure 3A,B) was selected. This V_HH was selected as (i) it

represents a classical length of CDRs of V_HH and (ii) it was experimentally used as a concrete case for comparison with the V_H of V_H-V_L complexes.

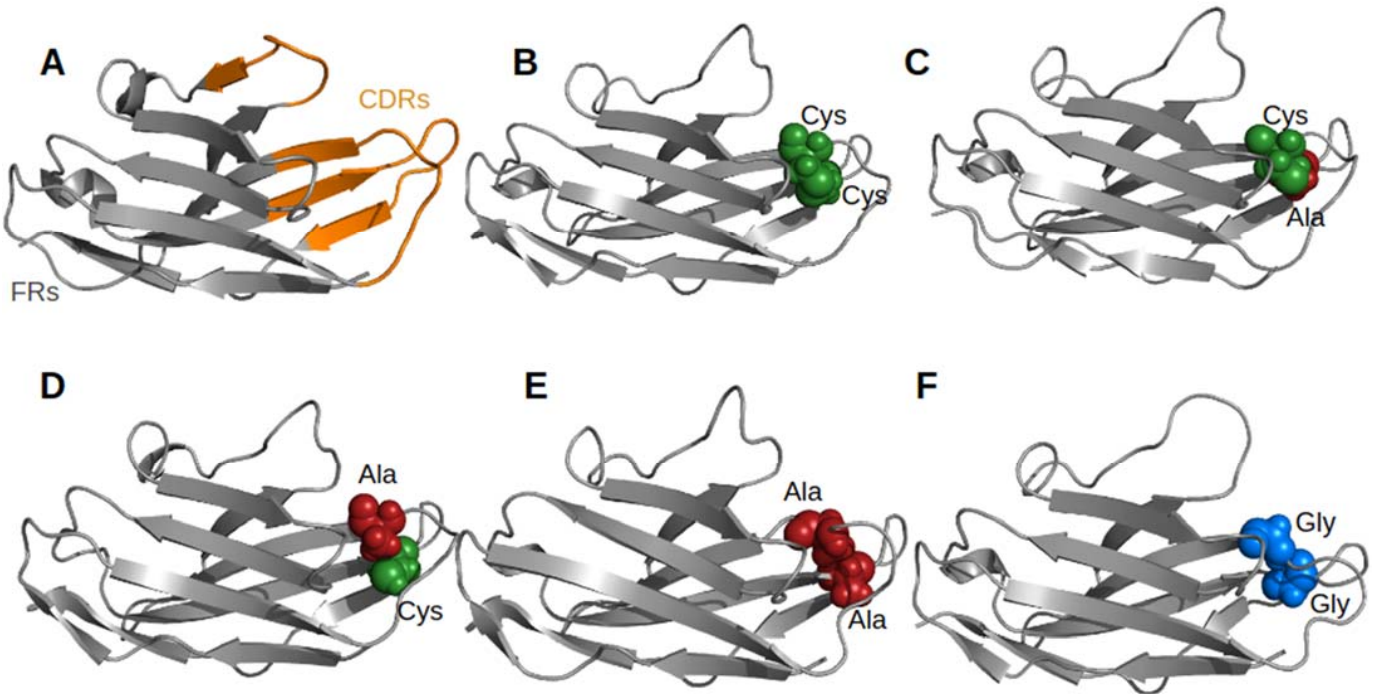

Figure 3. V_HH structure and the 2nd disulphide bridge. (**A**) FRs (in grey) and CDRs (in orange) delimitation, (**B**) wild type, (**C**–**F**) mutants. In (**C**,**D**) single and (**E**,**F**) double mutants, Cysteines are in green balls, Alanines in red, and Glycines in blue.

Single and double mutants have been built and examined to assess the effect of these mutations on the V_HH structure by molecular dynamics simulations. Four mutants were produced: two single mutants (32A-C99 and C32-99A, see Figure 3C,D) and two double mutants (32A-99A and 32G-99G, see Figure 3E,F). The Glycine double mutant aims to apprehend the impact of aliphatic chains on the V_HH structure.

2.2. Global Analyses

For all conditions, the root mean square deviation increases and reaches a plateau around 1 and 2 Å; similarly, the repetitive structures of FRs remain also quite constant during all simulations. The structures remain stable, and so simulations can be analysed. Figure 4A shown RMSF values. High values are associated, as expected, with CDRs (approximately at positions 23–37 and 50–63—it also encompasses the beginning of FR3- and 99–105). An increase in flexibility is observed for all mutants in the CDR1 region (going from the highest value of 2Å to 4Å for C32-99A and 32G-99G). An increase in flexibility is also observed in the CDR3 region for 32A-99A (and not 32G-99G). Surprisingly, a decrease in flexibility (RMSF value) is found for all mutants on CDR2. ΔRMSF (see Figure 4B) analysis emphasizes those differences. The second disulfide bridge seems to have an impact on the flexibility of each CDR and not on FRs. Indeed, its presence brings a greater rigidity in the CDR1 and CDR3 loop and would lead to a greater flexibility in CDR2.

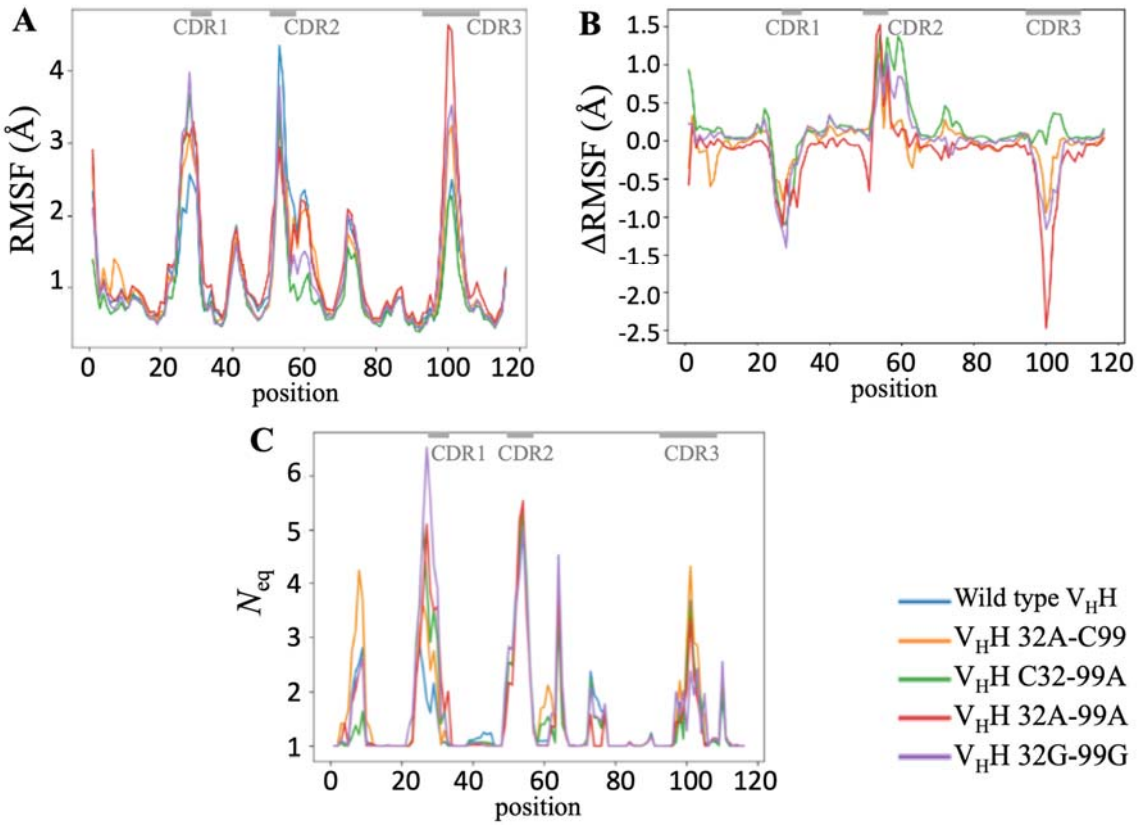

Figure 4. Changes in V_HH without the second disulphide bridge. (**A**) RMSF, (**B**) ΔRMSF, and (**C**) N_{eq} (PB entropy). Colours are (**A**,**C**) wild-type V_HH (blue), 32A-C99 (orange), C32-99A (green), 32A-99A (red), and 32G-99G (purple). The dashes at the top of each figure in grey represent the CDR positions.

2.3. Local Analyses

A more detailed analysis of flexibility is carried out by the use of Protein Blocks [50]. The N_{eq} analysis (see Figure 4C) provides a more complex and finest analysis [51–53]. A N_{eq} value of 1 means total rigidity, 4 is flexible, 6 is highly flexible, and 8 or more is a disordered region [54].

As for RMSF, CDR1 is considered to be going to a flexible conformation. The wild type has the lowest N_{eq} value of 3 (i.e., considered fairly flexible); all other systems see this value increase; and the extreme case is the double mutant 32G-99G which has a double value (a N_{eq} value of 6, i.e., highly flexible).

For CDR2, it is always highly flexible (with a common maximum N_{eq} value of 5). For all systems, as for RMSF, the beginning of FR3 (positions 58 to 63) is associated with a flexible N_{eq} value of 4. This FR is like most FRs strongly composed of β-strand, but this one is a very small β-strand and finished with a small helical zone (that could be considered a β-turn [55,56]). This region has the greatest flexibility (as seen in other systems [57]).

CDR3 has the least flexibility with N_{eq} values ranging between 2 and 4. Surprisingly, although it might be expected to be more flexible due to the absence of side chains, the most rigid system is the double mutant Glycine. The use of PBs also allows us to see that FR1 is slightly deformable with a max N_{eq} of 2 for wild type and of 4 for 32A-C99, when it is only 1.4 for C32-99A. Those results show that the second disulfide bond has an impact mainly on CDR1 deformability. Nonetheless, the limited effect on CDR3 is rather unexpected.

2.4. Comparison of Local Protein Conformations

To deepen the analysis of the local information used, ΔPB (a measure that quantifies the differences in PB frequency) can be used [58]. Analysis of ΔPB (see Figure 5A) allows for a finer description of the conformational diversity between wild-type and mutant

structures. ΔPB varies between 0, i.e., exact similar PB frequencies observed at the same position between two simulations, and 2, i.e., entirely different PB frequencies observed at the same position between two simulations.

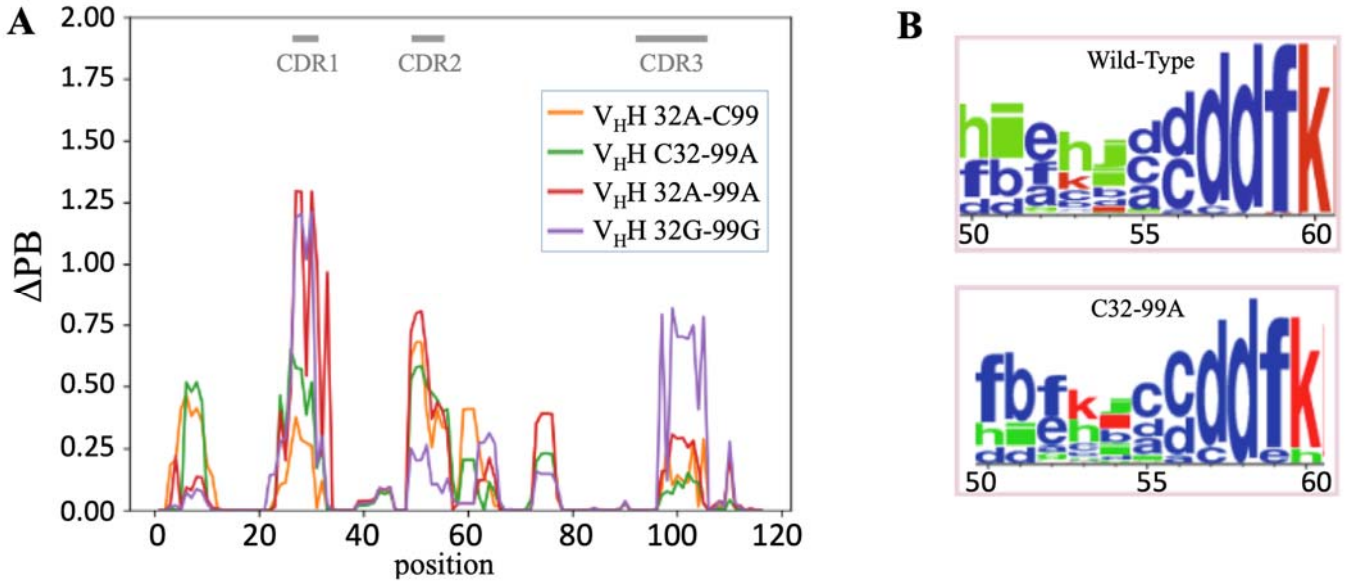

Figure 5. Local analyses. (**A**) ΔPB (difference in PB signature) between wild type and 32A-C99 (orange), C32-99A (green), 32A-99A (red), and 32G-99G (purple). The dashes at the top of each figure in grey represent the CDR positions. An example of the difference in the PBs of the wild-type and the 32A-C99 mutant is shown in (**B**) PB WebLogo [59] between positions 50 and 60.

FRs have a ΔPB value not exceeding 0.5 (one-quarter of PB occurrences are different). It is found for FR1 for 32A-C99 and C32-99A while double mutants have a wild-type-like PB signature for FR1. For FR3, few positions have ΔPB higher than 0.25 (1/8th of PB occurrence is different). In FR3, it concerns position 75, an Alanine, which is in direct contact with CDR1 N-ter. Hence, the loss of the disulphide bridge has a limited impact on FRs. The only unexpected case is found for the N-ter (position 8) of FR1 that is far from CDRs.

As expected, the ΔPB is higher for the CDRs. A first interesting point is that each system is particular and that single and double mutants do not have the same behaviours at all. The second point is that the ΔPB values are quite different for each CDR.

For CDR1, the maximal ΔPB values are 1.25 for both double mutants (32A-99A and 32G-99G), i.e., PB distinct distribution (65%), while they reach 0.60 for C32-99A and 0.30 for 32A-C99. The maximal ΔPB value for CDR2 is 0.75 for 32A-99A, 0.60 for 32A-C99, 0.50 for C32-99A, and only 0.25 for 32G-99G. For CDR3, it is again totally different, with a maximal ΔPB value for 32G-99G (0.75), while all the other systems have ΔPB values less than 0.25.

Every mutant system is not equivalent. Hence, C32-99A had maximal ΔPB values of 0.50 for FR1, CDR1, and CDR2 and 0.15 for CDR3. Its symmetrical 32A-C99 had similar slightly lower values (0.4 for FR1, 0.3 for CDR1, 0.6 for CDR2, and 0.25 for CDR3), making these two systems the least impacted. For the double mutants, the results were quite different, with a low impact on FR1 (maximal ΔPB values of 0.2 and 0.05, resp.), a strong impact on CDR 1 (1.25 for both), and completely opposite behaviour on CDR2 (0.75 and 0.20, resp.) and CDR3 (0.25 and 0.75, resp.). These results show that the number of mutations and the type of change have a direct impact on local conformations. Nonetheless, these effects do not add up.

Thus, we saw that a maximum of one-third of the local conformations were sampled differently for CDR2 and CDR3, and two-thirds were sampled differently for CDR1. This could seem important at first glance, but actually, the problem is more complex. Indeed,

Figure 5B shows PB distribution with WebLogo representation for positions spanning from 50 to 60 (i.e., CDR2). They are associated with ΔPB around 0.65, i.e., one-third of difference. However, no new PB appears. It is always the same PBs in one or another system, but with a clear change in frequencies. For instance, at positions 50–54, the majority PB series is *hieid* for the wild type while it is PB series *fbfklc* for 32A-C99 at the same positions. Hence, for each system, both PB word series are found but with a frequency inversion of the major word. This example is representative of all the CDRs behaviours. We have (i) a restricted number of protein local conformations, but (ii) mutation(s) does not make a new local conformation, only a change(s) in the conformer's occurrence, i.e., the difference in ΔPB. This analysis allows for a precise comparison of V_HH structures that can be considered similar but with small dynamic differences despite sequence differences. By consequence, it explains why the binding could remain similar regardless of the presence or absence of the second disulphide bridge.

3. Discussion

Analysis of V_HHs has revealed the presence of an additional disulphide bridge between CDR1 and CDR3 (see Figure 2) [36,37,41]. They can be seen in 25% of all V_HHs [13,42,43]. Different experiments underline that it was not as essential as expected for the specific properties of V_HHs [44–46], and this V_HH is an excellent representative of all these types of VHHs with an extra disulphide bridge. In order to understand its influence, a molecular dynamics study has been set up and analysed. MDs have shown its interest in analysing V_HH behaviours [43,57,60–74].

Long simulations followed by detailed analysis of the systems studied were carried out to achieve this. A variety of mutations have been used to consider the absence of the extra disulphide bridge, and the results of the analyses of these mutant systems are complex. Thus, single mutants behave more like the wild type than double mutants. Using classical approaches (i.e., RSMF), this study shows that the absence of the second disulphide bridge appears to destabilize the local conformations of V_HH. Nonetheless, further information can be obtained by analysing the ΔPBs.

All the analyses show the impact of the second disulfide bond's absence on the rigidity/flexibility of the three CDRs. A contrario, it is highly limited on CDR1 and CDR3, mainly changing some equilibrium between conformers. Thus, it appears that breaking the disulphide bridge does not significantly influence V_HH conformation. Interestingly, an impact on the CDR2 rigidification has been identified, i.e., an increase in deformability is also observed but with no real global consequences.

Hence, there is no exploration of new conformations but a change in the equilibrium between the different observed conformations. This explains why the interaction of V_HHs with or without this second bridge is not really affected, but their rigidity is slightly reduced. Therefore, the additional disulphide bridge does not seem to be an essential part.

Thus, this additional disulfide bond seems to not play a major role in the question of local and global conformations and just has a subtle impact on the occurrence of the observed conformers. A slight decrease in the thermodynamic stability of V_HH domains is often observed. The question remains as to the possible influence of the disulfide bond on the protein folding process, i.e., its kinetic effects. Recent studies confirmed that the thermal stability of V_HH actually reflects thermodynamic stabilities in a wide range of temperatures [75,76], as previously stated [77–79]. Since almost a quarter of V_HHs have this additional disulphide bond, it seems logical that this property should not be strongly affected, but it would be good to have experimental data, which are quite difficult to obtain.

Also, the thermal stability and global thermodynamic equilibrium of different V_HHs can be explained by a higher folding stability to all temperatures. This property is particularly true in working conditions of around 37 °C for a therapeutic V_HH. This work therefore allows us to see that this second disulfide bridge, present or absent, will not have too important consequences for the design of therapeutic V_HHs.

4. Materials and Methods

4.1. V_HH Structure

The structure of one representative V_HH with two disulphide bridges was downloaded from the Protein Data Bank website (https://www.rcsb.org, accessed 19 December 2023) [80], with PDB id 1YC7 [35]. Chain A was selected, with only the first residue not resolved. The position of the classical first disulphide bridge is between residues 22 and 95, and the position of the second disulphide bridge is between residues 32 and 99. The structure was analysed by classical approaches such as MolProbity [81] and visually with PyMOL 2.4.0 software (https://pymol.org/2/, accessed 29 August 2023) [10–12].

4.2. Molecular Dynamics

Molecular dynamics (MDs) simulations were performed using GROMACS 2021.4 software [82] with the CHARMM-36 force field [83], considering five different systems: (i) the initial PDB structure of the V_HH, i.e., C32-C99, (ii) the first single mutant with change in one Cysteine by an Alanine, i.e., C32A-C99 (for simplification, it will be noted 32A-C99), (iii) the second single mutant with change in the second Cysteine by an Alanine, i.e., C32-C99A (it will be noted C32-99A), (iv) the first double mutant with change in the two Cysteines by two Alanines, i.e., 32A-99A, and (v) the first double mutant with change in the two Cysteines by two Glycines, i.e., 32G-99G. Each structural system was energy-minimized for 500 steps of steepest descent and 500 steps of conjugate gradient using GROMACS suite. The V_HH structures were soaked in a rhombic dodecahedral simulation box with TIP3P water molecules. After that, charge neutralization was achieved by adding sodium and chloride ions with one atmosphere of pressure and 310 K of temperature to correspond with the experimental conditions.

The MDs protocol is standardized through our previous works [58,60,84]. After 1 nanosecond (nsec) of equilibration, each system was simulated through multiple classical independent production runs with 4 replicates of 250 nanoseconds as in [59]. The equilibration protocol consists of one step with an NVT system and three more with an NPT system (with position restraints on protein atoms). During the first step in NVT and the second step in NPT, the protein is totally constrained and unable to move, while the equilibration affects the water molecules. In the third and fourth step in NPT, the constraints on the protein are slowly released. Molecular conformations were saved every 100 picoseconds for downstream analysis. This produced 1 µs of MDs simulation for each system.

Trajectory analyses were carried out with the GROMACS software, in-house Python, and R scripts. Root mean square deviations (RMSDs) and root mean square fluctuations (RMSFs) were calculated on Cα atoms only.

4.3. MDs Analysis

The analysis of MDs was performed using classic tools, such as RMSD and RMSF, and other more innovative ones such as PBxplore [51], a tool developed within the team to analyse Protein Blocks throughout the MDs simulation. RMSD (root mean square deviation) quantifies structural variations during dynamics by comparing each frame to a reference structure; here, this is the starting frame. For each frame, an average of the differences between the reference positions and the positions of the current frame is taken in order to have an RMSD value per unit of time.

The RMSF (root mean square fluctuation) is similar to the RMSD, by determining the fluctuation of each residue following the same principle as for the RMSD, i.e., a comparison with a reference. But this time, it is the average position of each residue, calculated during the simulation time, and thus the measure of the difference between the current position and the average position in order to have a flexibility value per position.

The assignment of secondary structures was carried out using the Dictionary of Secondary Structure of Protein (DSSP) [85,86]. The DSSP provides eight states of description (α-helix, π-helix, 3_{10}-helix, β-strands, β-turns, bents, β-bridge, and coil). Thus, from the trajectory file generated by GROMACS, the DSSP assigns the secondary structure element

for each time interval. This analysis allows us to easily see the stability or not of the protein secondary structure elements as a function of time.

Protein Blocks (PBs) are a structural alphabet composed of 16 local prototypes [50,87,88]. Each specific PB is characterized by the φ, and ψ dihedral angles of five consecutive residues with each PB assignment are focused on the central residue. Obtained through an unsupervised training approach and performed on a representative non-redundant databank, PBs give a reasonable approximation of all local protein 3D structures [89]. PBs are very efficient at tasks such as protein superimpositions [90,91] and MDs analyses [54,92–94]. They are labelled from *a* to *p*: PBs *m* and *d* can be roughly described as prototypes for α-helix and central β-strand, respectively. PBs *a* to *c* primarily represent β-strand N-caps and PBs *e* and *f* representing β-strand C-caps; PBs *a* to *j* are specific to coils, PBs *k* and *l* are specific to α-helix N-caps, while PBs *n* to *p* are specific to α-helix C-caps. PB assignment was carried out using our PBxplore tool (https://github.com/pierrepo/PBxplore, accessed 19 May 2024) [51].

PB assignments are carried out for each residue of the C-domain and over every snapshot extracted from MDs simulations. The equivalent number of PBs (N_{eq}) is a statistical measurement similar to entropy that represents the average number of PBs for a residue at a given position. N_{eq} is calculated as follows [50]:

$$N_{\mathrm{eq}} = \exp\left(-\sum_{x=1}^{16} f_x \ln f_x\right)$$

where f_x is the probability of PB x. A N_{eq} value of 1 indicates that only one type of PB is observed, while a value of 16 is equivalent to a random distribution. To underline the main differences between one system and another one for each position, the absolute difference ΔN_{eq} between corresponding N_{eq}s values was computed.

However, since the same ΔN_{eq} value can be obtained with different types of blocks in similar proportions, we have defined a complementary measure, ΔPB, that evaluates a change in PB profile by calculating the absolute sum of the differences for each PB between the probabilities of a PB x to be present in the first and the second forms (x goes from PB *a* to PB *p*). ΔPB is calculated as follows [59]:

$$\Delta\mathrm{PB} = \sum_{x=1}^{16} \left| \left(f_x^1 - f_x^2 \right) \right|$$

where f_x^1 and f_x^2 are the percentages of the occurrence of a PB x in the first and the second system, respectively. A value of 0 indicates perfect PBs identity between the 1st and 2nd systems, while a score of 2 indicates a maximum total difference.

PBxplore also uses WebLogo to provide a dedicated PB logo output [59].

Author Contributions: Conceptualization, A.G.d.B.; methodology, F.G., A.A.N., J.D. and A.G.d.B.; simulations, C.M.; formal analysis, J.D. and A.G.d.B.; resources, C.M., J.D. and A.G.d.B.; data curation, C.M.; writing—original draft preparation, C.M. and A.G.d.B.; writing—review and editing, C.M., F.G., A.A.N., J.D. and A.G.d.B.; visualization, A.A.N. and C.M.; supervision, A.A.N. and A.G.d.B.; project administration, A.G.d.B.; funding acquisition, F.G. and A.G.d.B. All authors have read and agreed to the published version of the manuscript.

Funding: This research was funded by the POE FEDER 2014-20 of the Conseil Régional de La Réunion (S3D VHH program, N° SYNERGIE RE0022962), EU-H2020, and Université de la Réunion. This work was supported by grants from the Ministry of Research (France), Université Paris Cité (formerly University Paris Diderot, Sorbonne Paris Cité, France and formerly Université de Paris), Université de la Réunion, National Institute for Blood Transfusion (INTS, France), National Institute for Health and Medical Research (INSERM, France), IdEx ANR-18-IDEX-0001, and labex GR-Ex. The labex GR-Ex, reference ANR-11-LABX-0051, is funded by the program "Investissements d'avenir" of the French National Research Agency, reference ANR-11-IDEX-0005-02. A.G.d.B. acknowledges GR-Ex 2023 grant. A.G.d.B. acknowledges Indo-French Centre for the Promotion of Advanced

Research/CEFIPRA for collaborative grant (number 5302-2). A.G.d.B. and J.D. acknowledge the French National Research Agency with grant ANR-19-CE17-0021 (BASIN). A.G.d.B. acknowledges the PHC CEDRE with grant 47811WM. A.A.N. acknowledges granted access to high-performance computing (HPC) resources at the French National Computing Centre CINES under grants no. AP010312904 (Occigen) and A0110313007 (Irene) funded by the GENCI (Grand Equipement National de Calcul Intensif).

Institutional Review Board Statement: Not applicable.

Informed Consent Statement: Not applicable.

Data Availability Statement: Molecular dynamics trajectories are available on request.

Acknowledgments: We would like to thank Catherine Etchebest, Jean-Christophe Gelly, Ragousandirane Radjasandirane, Frédéric Guyon, Frédéric Cadet, Philippe Charton, Adam Bellaïche, Ilyas Grandguillaume, Lucas Rouaud, Thomas Bailly, Carolynn Hierso, Poonam Vishwakarma, Akhila Melarkode Vattekatte, and Anne-Elizabeth Molza for fruitful discussions, Gabriel Cretin for various technical support, and Simon Forestier, Lynda Saminadin, Damien Guimond, and Juan-Manuel Mora-Rey for administrative support. We also thank Snoopy the wirehaired dachshund for his cooperation in these studies.

Conflicts of Interest: The authors declare no conflicts of interest. The funders had no role in the design of the study; in the collection, analyses, or interpretation of the data; in the writing of the manuscript, or in the decision to publish the results.

References

1. Hamers-Casterman, C.; Atarhouch, T.; Muyldermans, S.; Robinson, G.; Hamers, C.; Songa, E.B.; Bendahman, N.; Hamers, R. Naturally occurring antibodies devoid of light chains. *Nature* **1993**, *363*, 446–448. [CrossRef] [PubMed]
2. Roovers, R.C.; van Dongen, G.A.; van Bergen en Henegouwen, P.M. Nanobodies in therapeutic applications. *Curr. Opin. Mol. Ther.* **2007**, *9*, 327–335. [PubMed]
3. Siontorou, C.G. Nanobodies as novel agents for disease diagnosis and therapy. *Int. J. Nanomed.* **2013**, *8*, 4215–4227. [CrossRef]
4. Wernery, U. Camelid immunoglobulins and their importance for the new-born—A review. *J. Vet. Med. Ser. B Infect. Dis. Vet. Public Health* **2001**, *48*, 561–568.
5. Janssens, R.; Dekker, S.; Hendriks, R.W.; Panayotou, G.; van Remoortere, A.; San, J.K.; Grosveld, F.; Drabek, D. Generation of heavy-chain-only antibodies in mice. *Proc. Natl. Acad. Sci. USA* **2006**, *103*, 15130–15135. [CrossRef]
6. De Genst, E.; Saerens, D.; Muyldermans, S.; Conrath, K. Antibody repertoire development in camelids. *Dev. Comp. Immunol.* **2006**, *30*, 187–198. [CrossRef]
7. Omidfar, K.; Rasaee, M.J.; Kashanian, S.; Paknejad, M.; Bathaie, Z. Studies of thermostability in camelus bactrianus (bactrian camel) single-domain antibody specific for the mutant epidermal-growth-factor receptor expressed by pichia. *Biotechnol. Appl. Biochem.* **2007**, *46*, 41–49. [CrossRef] [PubMed]
8. Jin, B.K.; Odongo, S.; Radwanska, M.; Magez, S. Nanobodies®: A review of diagnostic and therapeutic applications. *Int. J. Mol. Sci.* **2023**, *24*, 5994. [CrossRef]
9. Tanaka, T.; Lobato, M.N.; Rabbitts, T.H. Single domain intracellular antibodies: A minimal fragment for direct in vivo selection of antigen-specific intrabodies. *J. Mol. Biol.* **2003**, *331*, 1109–1120. [CrossRef]
10. Delano, W.L. The Pymol Molecular Graphics System on World Wide Web. 2013. Available online: http://www.pymol.org (accessed on 11 February 2022).
11. *The Pymol Molecular Graphics System*, version 1.7.2.2; Schrödinger, LLC: New York, NY, USA, 2015.
12. *Pymol*, version 2.4.0; Schrödinger, LLC: New York, NY, USA, 2020.
13. Mitchell, L.S.; Colwell, L.J. Comparative analysis of nanobody sequence and structure data. *Proteins* **2018**, *86*, 697–706. [CrossRef]
14. Guilbaud, A.; Pecorari, F. Construction of synthetic VHH libraries in ribosome display format. *Methods Mol. Biol.* **2023**, *2681*, 19–31. [PubMed]
15. De Greve, H. Production of designer VHH-based antibodies in plants. *Methods Mol. Biol.* **2022**, *2446*, 205–230. [PubMed]
16. Asada, T.; Takagi, D.; Nakai, M.; Abe, S.; Yuasa, K. Secretory production of a camelid single-domain antibody (VHH, nanobody) by the *Serratia marcescens* lip system in *Escherichia coli*. *Biochem. Biophys. Res. Commun.* **2021**, *549*, 105–112. [CrossRef]
17. Jia, Q.; Ren, H.; Zhang, S.; Yang, H.; Gao, S.; Fan, R. Preparation and application of *Clostridium perfringens* alpha toxin nanobodies. *Vet. Sci.* **2024**, *11*, 381. [CrossRef]
18. Saerens, D.; Pellis, M.; Loris, R.; Pardon, E.; Dumoulin, M.; Matagne, A.; Wyns, L.; Muyldermans, S.; Conrath, K. Identification of a universal VHH framework to graft non-canonical antigen-binding loops of camel single-domain antibodies. *J. Mol. Biol.* **2005**, *352*, 597–607. [CrossRef]
19. Wang, M.; Ying, T.; Wu, Y. Single-domain antibodies as therapeutics for solid tumor treatment. *Acta Pharm. Sin. B* **2024**, *14*, 2854–2868. [CrossRef]

20. Kinoshita, S.; Nakakido, M.; Mori, C.; Kuroda, D.; Caaveiro, J.M.M.; Tsumoto, K. Molecular basis for thermal stability and affinity in a VHH: Contribution of the framework region and its influence in the conformation of the CDR3. *Protein Sci. Publ. Protein Soc.* **2022**, *31*, e4450. [CrossRef] [PubMed]
21. Scully, M.; Cataland, S.R.; Peyvandi, F.; Coppo, P.; Knöbl, P.; Kremer Hovinga, J.A.; Metjian, A.; de la Rubia, J.; Pavenski, K.; Callewaert, F.; et al. Caplacizumab treatment for acquired thrombotic thrombocytopenic purpura. *N. Engl. J. Med.* **2019**, *380*, 335–346. [CrossRef]
22. Völker, L.A.; Kaufeld, J.; Balduin, G.; Merkel, L.; Kühne, L.; Eichenauer, D.A.; Osterholt, T.; Hägele, H.; Kann, M.; Grundmann, F.; et al. Impact of first-line use of caplacizumab on treatment outcomes in immune thrombotic thrombocytopenic purpura. *J. Thromb. Haemost.* **2023**, *21*, 559–572. [CrossRef]
23. Scully, M.; de la Rubia, J.; Pavenski, K.; Metjian, A.; Knöbl, P.; Peyvandi, F.; Cataland, S.; Coppo, P.; Kremer Hovinga, J.A.; Minkue Mi Edou, J.; et al. Long-term follow-up of patients treated with caplacizumab and safety and efficacy of repeat caplacizumab use: Post-hercules study. *J. Thromb. Haemost.* **2022**, *20*, 2810–2822. [CrossRef]
24. Keam, S.J. Ozoralizumab: First approval. *Drugs* **2023**, *83*, 87–92. [CrossRef] [PubMed]
25. Tanaka, Y.; Miyazaki, Y.; Kawanishi, M.; Yamasaki, H.; Takeuchi, T. Long-term safety and efficacy of anti-TNF multivalent VHH antibodies ozoralizumab in patients with rheumatoid arthritis. *RMD Open* **2024**, *10*, e004480. [CrossRef] [PubMed]
26. Zhao, W.H.; Wang, B.Y.; Chen, L.J.; Fu, W.J.; Xu, J.; Liu, J.; Jin, S.W.; Chen, Y.X.; Cao, X.M.; Yang, Y.; et al. Four-year follow-up of LCAR-B38M in relapsed or refractory multiple myeloma: A phase 1, single-arm, open-label, multicenter study in china (LEGEND-2). *J. Hematol. Oncol.* **2022**, *15*, 86. [CrossRef]
27. Mullard, A. FDA approves second BCMA-targeted CAR-T cell therapy. *Nat. Rev. Drug Discov.* **2022**, *21*, 249. [CrossRef] [PubMed]
28. Milstein, C. The disulphide bridges of immunoglobulin kappa-chains. *Biochem. J.* **1966**, *101*, 338–351. [CrossRef]
29. Pinck, J.R.; Milstein, C. Disulphide bridges of a human immunoglobulin g protein. *Nature* **1967**, *216*, 941–942. [CrossRef] [PubMed]
30. Edelman, G.M.; Cunningham, B.A.; Gall, W.E.; Gottlieb, P.D.; Rutishauser, U.; Waxdal, M.J. The covalent structure of an entire gammag immunoglobulin molecule. *Proc. Natl. Acad. Sci. USA* **1969**, *63*, 78–85. [CrossRef]
31. Amzel, L.M.; Poljak, R.J. Three-dimensional structure of immunoglobulins. *Annu. Rev. Biochem.* **1979**, *48*, 961–997. [CrossRef]
32. Proba, K.; Honegger, A.; Plückthun, A. A natural antibody missing a cysteine in VH: Consequences for thermodynamic stability and folding. *J. Mol. Biol.* **1997**, *265*, 161–172. [CrossRef]
33. Lefranc, M.P.; Pommié, C.; Kaas, Q.; Duprat, E.; Bosc, N.; Guiraudou, D.; Jean, C.; Ruiz, M.; Da Piédade, I.; Rouard, M.; et al. IMGT unique numbering for immunoglobulin and T cell receptor constant domains and Ig superfamily C-like domains. *Dev. Comp. Immunol.* **2005**, *29*, 185–203. [CrossRef]
34. Liu, H.; May, K. Disulfide bond structures of IgG molecules: Structural variations, chemical modifications and possible impacts to stability and biological function. *mAbs* **2012**, *4*, 17–23. [CrossRef] [PubMed]
35. Conrath, K.; Vincke, C.; Stijlemans, B.; Schymkowitz, J.; Decanniere, K.; Wyns, L.; Muyldermans, S.; Loris, R. Antigen binding and solubility effects upon the veneering of a camel VHH in framework-2 to mimic a VH. *J. Mol. Biol.* **2005**, *350*, 112–125. [CrossRef]
36. Nguyen, V.K.; Hamers, R.; Wyns, L.; Muyldermans, S. Camel heavy-chain antibodies: Diverse germline VHH and specific mechanisms enlarge the antigen-binding repertoire. *EMBO J.* **2000**, *19*, 921–930. [CrossRef]
37. Conrath, K.E.; Wernery, U.; Muyldermans, S.; Nguyen, V.K. Emergence and evolution of functional heavy-chain antibodies in camelidae. *Dev. Comp. Immunol.* **2003**, *27*, 87–103. [CrossRef] [PubMed]
38. Eskier, N.E.; Eskier, D.; Firuzan, E.; Uzunlar, S.K. Physicochemical differences between camelid single-domain antibodies and mammalian antibodies. *Turk. J. Biol.* **2023**, *47*, 423–436. [CrossRef]
39. Liu, Y.; Yi, L.; Li, Y.; Wang, Z.; Jirimutu. Characterization of heavy-chain antibody gene repertoires in bactrian camels. *J. Genet. Genom.* **2023**, *50*, 38–45. [CrossRef]
40. Xu, M.; Zhao, Z.; Deng, P.; Sun, M.; Chiu, C.K.C.; Wu, Y.; Wang, H.; Bi, Y. Functional divergence in the affinity and stability of non-canonical cysteines and non-canonical disulfide bonds: Insights from a VHH and VNAR study. *Int. J. Mol. Sci.* **2024**, *25*, 9801. [CrossRef] [PubMed]
41. Harmsen, M.M.; Ruuls, R.C.; Nijman, I.J.; Niewold, T.A.; Frenken, L.G.; de Geus, B. Llama heavy-chain V regions consist of at least four distinct subfamilies revealing novel sequence features. *Mol. Immunol.* **2000**, *37*, 579–590. [CrossRef]
42. Li, X.; Duan, X.; Yang, K.; Zhang, W.; Zhang, C.; Fu, L.; Ren, Z.; Wang, C.; Wu, J.; Lu, R.; et al. Comparative analysis of immune repertoires between bactrian camel's conventional and heavy-chain antibodies. *PLoS ONE* **2016**, *11*, e0161801. [CrossRef]
43. Melarkode Vattekatte, A.; Shinada, N.K.; Narwani, T.J.; Noel, F.; Bertrand, O.; Meyniel, J.P.; Malpertuy, A.; Gelly, J.C.; Cadet, F.; de Brevern, A.G. Discrete analysis of camelid variable domains: Sequences, structures, and in-silico structure prediction. *PeerJ* **2020**, *8*, e8408. [CrossRef]
44. Mendoza, M.N.; Jian, M.; King, M.T.; Brooks, C.L. Role of a noncanonical disulfide bond in the stability, affinity, and flexibility of a VHH specific for the *Listeria* virulence factor InlB. *Protein Sci.* **2020**, *29*, 1004–1017. [CrossRef]
45. Liu, H.; Schittny, V.; Nash, M.A. Removal of a conserved disulfide bond does not compromise mechanical stability of a VHH antibody complex. *Nano Lett.* **2019**, *19*, 5524–5529. [CrossRef] [PubMed]
46. Ma, H.; Ó'Fágáin, C.; O'Kennedy, R. Antibody stability: A key to performance—Analysis, influences and improvement. *Biochimie* **2020**, *177*, 213–225. [CrossRef]
47. Thornton, J.M. Disulphide bridges in globular proteins. *J. Mol. Biol.* **1981**, *151*, 261–287. [CrossRef]

48. Thangudu, R.R.; Manoharan, M.; Srinivasan, N.; Cadet, F.; Sowdhamini, R.; Offmann, B. Analysis on conservation of disulphide bonds and their structural features in homologous protein domain families. *BMC Struct. Biol.* **2008**, *8*, 55. [CrossRef] [PubMed]
49. Govaert, J.; Pellis, M.; Deschacht, N.; Vincke, C.; Conrath, K.; Muyldermans, S.; Saerens, D. Dual beneficial effect of interloop disulfide bond for single domain antibody fragments. *J. Biol. Chem.* **2012**, *287*, 1970–1979. [CrossRef]
50. de Brevern, A.G.; Etchebest, C.; Hazout, S. Bayesian probabilistic approach for predicting backbone structures in terms of protein blocks. *Proteins* **2000**, *41*, 271–287. [CrossRef] [PubMed]
51. Barnoud, J.; Santuz, H.; Craveur, P.; Joseph, A.P.; Jallu, V.; de Brevern, A.G.; Poulain, P. Pbxplore: A tool to analyze local protein structure and deformability with protein blocks. *PeerJ* **2017**, *5*, e4013. [CrossRef]
52. Jallu, V.; Poulain, P.; Fuchs, P.F.; Kaplan, C.; de Brevern, A.G. Modeling and molecular dynamics of HPA-1a and -1b polymorphisms: Effects on the structure of the β3 subunit of the αiibβ3 integrin. *PLoS ONE* **2012**, *7*, e47304. [CrossRef]
53. Craveur, P.; Joseph, A.P.; Esque, J.; Narwani, T.J.; Noël, F.; Shinada, N.; Goguet, M.; Leonard, S.; Poulain, P.; Bertrand, O.; et al. Protein flexibility in the light of structural alphabets. *Front. Mol. Biosci.* **2015**, *2*, 20. [CrossRef]
54. Melarkode Vattekatte, A.; Narwani, T.J.; Floch, A.; Maljković, M.; Bisoo, S.; Shinada, N.K.; Kranjc, A.; Gelly, J.C.; Srinivasan, N.; Mitić, N.; et al. A structural entropy index to analyse local conformations in intrinsically disordered proteins. *J. Struct. Biol.* **2020**, *210*, 107464.
55. Venkatachalam, C.M. Stereochemical criteria for polypeptides and proteins. V. Conformation of a system of three linked peptide units. *Biopolymers* **1968**, *6*, 1425–1436. [CrossRef]
56. Venkatachalam, C.M.; Ramachandran, G.N. Conformation of polypeptide chains. *Annu. Rev. Biochem.* **1969**, *38*, 45–82. [CrossRef]
57. Vattekatte, A.M.; Diharce, J.; Rebehmed, J.; Cadet, F.; Gardebien, F.; Etchebest, C.; de Brevern, A.G. General trends of the *Camelidae* antibody V_HHs domain dynamics. *Int. J. Mol. Sci.* **2023**, *24*, 4511. [CrossRef]
58. Goguet, M.; Narwani, T.J.; Petermann, R.; Jallu, V.; de Brevern, A.G. In silico analysis of glanzmann variants of *Calf*-1 domain of $\alpha_{IIb}\beta_3$ integrin revealed dynamic allosteric effect. *Sci. Rep.* **2017**, *7*, 8001. [CrossRef]
59. Crooks, G.E.; Hon, G.; Chandonia, J.M.; Brenner, S.E. Weblogo: A sequence logo generator. *Genome Res.* **2004**, *14*, 1188–1190. [CrossRef]
60. Martins, C.; Diharce, J.; Nadaradjane, A.A.; de Brevern, A.G. Evaluation of the potential impact of in silico humanization on V_HH dynamics. *Int. J. Mol. Sci.* **2023**, *24*, 14586. [CrossRef] [PubMed]
61. Vishwakarma, P.; Vattekatte, A.M.; Shinada, N.; Diharce, J.; Martins, C.; Cadet, F.; Gardebien, F.; Etchebest, C.; Nadaradjane, A.A.; de Brevern, A.G. V_HH structural modelling approaches: A critical review. *Int. J. Mol. Sci.* **2022**, *23*, 3721. [CrossRef] [PubMed]
62. Melarkode Vattekatte, A.; Cadet, F.; Gelly, J.C.; de Brevern, A.G. Insights into comparative modeling of V_HH domains. *Int. J. Mol. Sci.* **2021**, *22*, 9771. [CrossRef]
63. Nadaradjane, A.A.; Diharce, J.; Rebehmed, J.; Cadet, F.; Gardebien, F.; Gelly, J.-C.; Etchebest, C.; de Brevern, A.G. Quality assessment of V_HH models. *JBSD* **2023**, *41*, 13287–133301. [CrossRef] [PubMed]
64. Verkhivker, G. Allosteric determinants of the SARS-CoV-2 spike protein binding with nanobodies: Examining mechanisms of mutational escape and sensitivity of the omicron variant. *Int. J. Mol. Sci.* **2022**, *23*, 2172. [CrossRef] [PubMed]
65. Verkhivker, G. Conformational flexibility and local frustration in the functional states of the SARS-CoV-2 spike B.1.1.7 and B.1.351 variants: Mutation-induced allosteric modulation mechanism of functional dynamics and protein stability. *Int. J. Mol. Sci.* **2022**, *23*, 1646. [CrossRef] [PubMed]
66. Omotuyi, O.; Olubiyi, O.; Nash, O.; Afolabi, E.; Oyinloye, B.; Fatumo, S.; Femi-Oyewo, M.; Bogoro, S. SARS-CoV-2 omicron spike glycoprotein receptor binding domain exhibits super-binder ability with ACE2 but not convalescent monoclonal antibody. *Comput. Biol. Med.* **2022**, *142*, 105226. [CrossRef]
67. Fernández-Quintero, M.L.; DeRose, E.F.; Gabel, S.A.; Mueller, G.A.; Liedl, K.R. Nanobody paratope ensembles in solution characterized by md simulations and nmr. *Int. J. Mol. Sci.* **2022**, *23*, 5419. [CrossRef]
68. Verkhivker, G.M.; Agajanian, S.; Oztas, D.Y.; Gupta, G. Atomistic simulations and in silico mutational profiling of protein stability and binding in the SARS-CoV-2 spike protein complexes with nanobodies: Molecular determinants of mutational escape mechanisms. *ACS Omega* **2021**, *6*, 26354–26371. [CrossRef]
69. Soler, M.A.; Medagli, B.; Wang, J.; Oloketuyi, S.; Bajc, G.; Huang, H.; Fortuna, S.; de Marco, A. Effect of humanizing mutations on the stability of the llama single-domain variable region. *Biomolecules* **2021**, *11*, 163. [CrossRef]
70. Ikeuchi, E.; Kuroda, D.; Nakakido, M.; Murakami, A.; Tsumoto, K. Delicate balance among thermal stability, binding affinity, and conformational space explored by single-domain V_HH antibodies. *Sci. Rep.* **2021**, *11*, 20624. [CrossRef]
71. Higashida, R.; Matsunaga, Y. Enhanced conformational sampling of nanobody CDR H3 loop by generalized replica-exchange with solute tempering. *Life* **2021**, *11*, 1428. [CrossRef] [PubMed]
72. Bekker, G.J.; Ma, B.; Kamiya, N. Thermal stability of single-domain antibodies estimated by molecular dynamics simulations. *Protein Sci.* **2019**, *28*, 429–438. [CrossRef]
73. Su, Z.Y.; Wang, Y.T. A molecular dynamics simulation of the human lysozyme—Camelid VHH HL6 antibody system. *Int. J. Mol. Sci.* **2009**, *10*, 1719–1727. [CrossRef]
74. Hasannejad-Asl, B.; Hashemzadeh, H.; Pooresmaeil, F.; Dabiri, M.; Pooresmaeil, M.-R.; Ahmadvand, D.; Hosseini, A. Molecular dynamics simulation of the brain-isolated single-domain antibody/nanobody from camels through in vivo phage display screening. *Front. Mol. Biosci.* **2024**, *11*, 1414119. [CrossRef]

75. Gómez-Mulas, A.; Salido, E.; Pey, A.L. Thermodynamic versus kinetic basis for the high conformational stability of nanobodies for therapeutic applications. *bioRxiv* **2024**. [CrossRef]
76. Kunz, P. Assessing the aggregation propensity of single-domain antibodies upon heat-denaturation employing the ΔT_m shift. *Methods Mol. Biol.* **2022**, *2446*, 233–244. [PubMed]
77. Dumoulin, M.; Conrath, K.; Van Meirhaeghe, A.; Meersman, F.; Heremans, K.; Frenken, L.G.; Muyldermans, S.; Wyns, L.; Matagne, A. Single-domain antibody fragments with high conformational stability. *Protein Sci.* **2002**, *11*, 500–515. [CrossRef]
78. Pérez, J.M.; Renisio, J.G.; Prompers, J.J.; van Platerink, C.J.; Cambillau, C.; Darbon, H.; Frenken, L.G. Thermal unfolding of a llama antibody fragment: A two-state reversible process. *Biochemistry* **2001**, *40*, 74–83. [CrossRef] [PubMed]
79. Kunz, P.; Flock, T.; Soler, N.; Zaiss, M.; Vincke, C.; Sterckx, Y.; Kastelic, D.; Muyldermans, S.; Hoheisel, J.D. Exploiting sequence and stability information for directing nanobody stability engineering. *Biochim. Biophys. Acta Gen. Subj.* **2017**, *1861*, 2196–2205. [CrossRef]
80. Berman, H.M.; Westbrook, J.; Feng, Z.; Gilliland, G.; Bhat, T.N.; Weissig, H.; Shindyalov, I.N.; Bourne, P.E. The protein data bank. *Nucleic Acids Res.* **2000**, *28*, 235–242. [CrossRef]
81. Williams, C.J.; Headd, J.J.; Moriarty, N.W.; Prisant, M.G.; Videau, L.L.; Deis, L.N.; Verma, V.; Keedy, D.A.; Hintze, B.J.; Chen, V.B.; et al. Molprobity: More and better reference data for improved all-atom structure validation. *Protein Sci.* **2018**, *27*, 293–315. [CrossRef]
82. Van Der Spoel, D.; Lindahl, E.; Hess, B.; Groenhof, G.; Mark, A.E.; Berendsen, H.J. Gromacs: Fast, flexible, and free. *J. Comput. Chem.* **2005**, *26*, 1701–1718. [CrossRef]
83. Huang, J.; MacKerell, A.D., Jr. CHARMM36 all-atom additive protein force field: Validation based on comparison to NMR data. *J. Comput. Chem.* **2013**, *34*, 2135–2145. [CrossRef]
84. Narwani, T.J.; Craveur, P.; Shinada, N.K.; Floch, A.; Santuz, H.; Vattekatte, A.M.; Srinivasan, N.; Rebehmed, J.; Gelly, J.C.; Etchebest, C.; et al. Discrete analyses of protein dynamics. *J. Biomol. Struct. Dyn.* **2020**, *38*, 2988–3002. [CrossRef] [PubMed]
85. Kabsch, W.; Sander, C. Dictionary of protein secondary structure: Pattern recognition of hydrogen-bonded and geometrical features. *Biopolymers* **1983**, *22*, 2577–2637. [CrossRef] [PubMed]
86. Touw, W.G.; Baakman, C.; Black, J.; te Beek, T.A.; Krieger, E.; Joosten, R.P.; Vriend, G. A series of pdb-related databanks for everyday needs. *Nucleic Acids Res.* **2015**, *43*, D364–D368. [CrossRef]
87. de Brevern, A.G. Analysis of protein disorder predictions in the light of a protein structural alphabet. *Biomolecules* **2020**, *10*, 1080. [CrossRef]
88. Offmann, B.; Tyagi, M.; de Brevern, A.G. Local protein structures. *Curr. Bioinform.* **2007**, *3*, 165–202. [CrossRef]
89. Joseph, A.P.; Agarwal, G.; Mahajan, S.; Gelly, J.C.; Swapna, L.S.; Offmann, B.; Cadet, F.; Bornot, A.; Tyagi, M.; Valadié, H. A short survey on protein blocks. *Biophys. Rev.* **2010**, *2*, 137–145. [CrossRef]
90. Joseph, A.P.; Srinivasan, N.; de Brevern, A.G. Improvement of protein structure comparison using a structural alphabet. *Biochimie* **2011**, *93*, 1434–1445. [CrossRef]
91. Léonard, S.; Joseph, A.P.; Srinivasan, N.; Gelly, J.C.; de Brevern, A.G. Mulpba: An efficient multiple protein structure alignment method based on a structural alphabet. *J. Biomol. Struct. Dyn.* **2014**, *32*, 661–668. [CrossRef] [PubMed]
92. Radjasandirane, R.; de Brevern, A.G. Structural and dynamic differences between calreticulin mutants associated with essential thrombocythemia. *Biomolecules* **2023**, *13*, 509. [CrossRef]
93. Vander Meersche, Y.; Cretin, G.; Gheeraert, A.; Gelly, J.C.; Galochkina, T. ATLAS: Protein flexibility description from atomistic molecular dynamics simulations. *Nucleic Acids Res.* **2024**, *52*, D384–D392. [CrossRef]
94. Ladislav, M.; Cerny, J.; Krusek, J.; Horak, M.; Balik, A.; Vyklicky, L. The LILI motif of M3-S2 linkers is a component of the NMDA receptor channel gate. *Front. Mol. Neurosci.* **2018**, *11*, 113. [CrossRef] [PubMed]